ELSEVIER

Journal of Alloys and Compounds 275–277 (1998) 154–160

Journal of ALLOYS AND COMPOUNDS

# Electronic and magnetic properties of the 4f and 5f intermetallics from Mössbauer spectroscopy

J.P. Sanchez[a,*], E. Colineau[a], P. Vulliet[a,b], K. Tomala[c]

[a]*Département de Recherche Fondamentale sur la Matière Condensée, SPSMS, CEA-Grenoble, 17 rue des Martyrs, 38054 Grenoble cedex 9, France*
[b]*Université Joseph Fourier, B.P. 53, 38041 Grenoble cedex 9, France*
[c]*Institute of Physics, Jagiellonian University, Krakow, Poland*

**Abstract**

Over the years Mössbauer spectroscopy has proved to be an important tool for the study of f-electron systems. Through measurements of the hyperfine interactions, this microscopic technique gives access to the charge state of the resonant atom (isomer shift), to its local symmetry (quadrupole splitting) and to the magnetic moment associated with its open electron shells (magnetic splitting). With the help of a few examples taken from recent work we demonstrate the power of this technique for obtaining information on the electronic and magnetic properties of 4f and 5f intermetallics. © 1998 Elsevier Science S.A.

*Keywords:* Electronic and magnetic properties; Magnetic superconductors; Mössbauer spectroscopy; Multilayers; Neptunium compounds; Rare-earth intermetallics

## 1. Introduction

Mössbauer spectroscopy, through measurements of hyperfine parameters, is a well established microscopic tool for gaining information on the electronic and magnetic properties of rare-earth (R) and actinide (An) systems [1,2]. The properties of 4f compounds (except for anomalous rare earths such as Ce, Yb, etc.) are generally well understood in the framework of localized models [3,4]. The situation in 5f systems is far more complex [5,6]. Over the years, the central question has remained the 3d-like itinerant (band) versus 4f-like localized electron behaviour of the 5f electrons in actinide systems.

The bulk of the work recently devoted to 4f systems is essentially related to the determination of the basic properties of new series of materials with some of them suitable for application (permanent magnets, magnetic recording, superconductors). By contrast, those dealing with neptunium systems ($^{237}$Np is the only popular Mössbauer probe among the actinides) focus mainly on a better understanding of their exotic properties (e.g., heavy fermion and Kondo lattice behaviour [7,8]), also encountered in anomalous rare earths [9–11], i.e. in strongly correlated electron systems.

Here we will illustrate using specific examples the impact of Mössbauer spectroscopy in rare earth and actinide research. Results obtained for the new quaternary magnetic superconductors ($RNi_2B_2C$) and for Dy–Fe multilayers will be discussed. Special emphasis will be given to cubic ($AuCu_3$-type) $NpX_3$ compounds whose magnetic properties span a large range of behaviour: non-magnetic ($NpGe_3$), localized magnets ($NpAl_3$, $NpGa_3$, $NpIn_3$), and ordered Kondo lattice ($NpSn_3$). These results will be compared with those obtained earlier for the ''less magnetic'' $UX_3$ analogs.

## 2. Mössbauer spectroscopy

Unlike Ce, all rare earths possess at least one Mössbauer transition. However, only a few of them are suitable for systematic investigations. Extensive studies of 4f systems have been carried out for Eu, Gd, Dy, Er, Tm and Yb. Within the actinides, systematic data exist only for Np, although Am possesses a suitable Mössbauer isotope ($^{243}$Am). Information on the electronic and magnetic properties is provided by the hyperfine interaction parameters.

The isomer shift ($\delta_{IS}$) is related to the electronic charge density $\rho(0)$ inside the Mössbauer probe nucleus. Changes in isomer shift arise either from a direct contribution of

*Corresponding author. Fax: +33 04 76 88 51 09; e-mail: jsanchez@cea.fr


PII: S0925-8388(98)00294-1

valence s and relativistic $p_{1/2}$ electrons or from the shielding effects of valence electrons of $p_{3/2}$, d and f character. Removal of d or f electrons increases $\rho(0)$, whereas the removal of s ($p_{1/2}$) electrons decreases $\rho(0)$. For a given charge state, it is generally accepted that covalency effects produce a decrease of $\rho(0)$ while conduction electrons lead to an increase of $\rho(0)$. It is worth mentioning that isomer shift measurements have played a central role in the determination of the mean valence of Eu in mixed-valence Eu systems [12] and of the electron configuration of Np ions in actinide intermetallics [1,2].

The quadrupole interaction is related to the electric field gradient (efg) at the nucleus created by the open f-shell (valence contribution) and the non-spherical ionic charge distributions on surrounding lattice sites. In non-S state ions the former contribution, proportional to $\langle 3J_z^2 - J(J+1)\rangle$, generally dominates. It is associated with the ground and populated excited states wave functions of the f ions (Table 1). In S-state ions (e.g., $Gd^{3+}$), the valence contribution vanishes. As shown below, the lattice efg measured in Gd intermetallics has been used extensively to evaluate the second-order ($B_2^0$) crystal electric field (CEF) parameter in isostructural series of rare-earth intermetallics.

The magnetic hyperfine field extracted from the Zeeman splitting of the Mössbauer spectra arises from different contributions. In S-state ions the field is due mainly to the contact term (core polarization field). In non S-state ions (i.e. those having an orbital angular momentum $L \neq 0$), the hyperfine field is essentially due to the open f-shell contribution (orbital and spin dipolar fields). In heavy rare earths, the spin orbit coupling ($\mathcal{H}_{SO}$) dominates the crystal field ($\mathcal{H}_{CEF}$) as well as the exchange interactions $\mathcal{H}_{EX}$. Furthermore, in most cases $\mathcal{H}_{EX}$ exceeds $\mathcal{H}_{CEF}$. Thus, the hyperfine field proportional to $g_J\langle J_z\rangle$ often attains the free-ion value ($\langle J_z\rangle = J$); see Table 1. In the actinides, $\mathcal{H}_{SO} \approx \mathcal{H}_{CEF} \approx \mathcal{H}_{EX}$, neither $J$ nor $J_z$ are necessarily good quantum numbers. Nevertheless, a simple linear relation ($H_{hf}/m = 215T/\mu_B$) between the Np hyperfine field ($H_{hf}$) and the magnetic moment ($m$) determined by neutron diffraction holds even for itinerant magnets. Note that any reduction of $H_{hf}$ with respect to the maximum free-ion value in anomalous rare-earth and actinide intermetallics is either due to crystal field quenching or (and) Kondo screening of the magnetic moment.

Table 1
Free-ion ($J_z = J$) hyperfine field ($H_{hf}$) and quadrupole coupling constant ($e^2qQ$) for rare earths and actinides of interest

| Ion | Configuration | $H_{hf}$ (T) | $e^2qQ$ (mm s$^{-1}$) |
|---|---|---|---|
| $Eu^{3+}$ | $4f^6:{}^7F_0$ | 0 | 0 |
| $Eu^{2+}$ | $4f^7:{}^8S_{7/2}$ | −34 | 0 |
| $Gd^{3+}$ | $4f^7:{}^8S_{7/2}$ | −34 | 0 |
| $Dy^{3+}$ | $4f^9:{}^6H_{15/2}$ | 569 | 135 |
| $Er^{3+}$ | $4f^{11}:{}^4I_{15/2}$ | 765 | 16.3 |
| $Tm^{3+}$ | $4f^{12}:{}^3H_6$ | 662 | 316.4 |
| $Yb^{3+}$ | $4f^{13}:{}^2F_{7/2}$ | 411 | 47.2 |
| $Yb^{2+}$ | $4f^{14}:{}^1S_0$ | 0 | 0 |
| $Np^{3+}$ | $5f^4:{}^5I_4$ | 530 | −27.3 |
| $Np^{4+}$ | $5f^3:{}^4I_{9/2}$ | 590 | 32.3 |

## 3. Mössbauer study of the quaternary magnetic superconductors $RNi_2B_2C$

The properties of the new class of quaternary rare-earth borocarbides $RNi_2B_2C$ which crystallize in the body centred tetragonal structure (*I4/mmm* space group) have attracted much interest because in some members of this series (R = Dy, Ho, Er, Tm), superconductivity ($T_C \approx 6$–11 K) and antiferromagnetic order ($T_N \approx 1.5$–11 K) coexist with comparable critical temperatures in contrast to ternary Chevrel phases or high-$T_C$ cuprates [13]. The highest Néel temperature (20 K) is observed for $GdNi_2B_2C$, as expected if the dominant exchange interactions are of the RKKY-type. Although this latter compound is non-superconducting, its Mössbauer study provided unique information (second-order $B_2^0$ crystal field parameter across the rare-earth series, magnetic structure).

### 3.1. $GdNi_2B_2C$

This compound orders antiferromagnetically at ≈20 K and undergoes a second magnetic phase transition at ~14 K [14]. Because of the high absorption cross section of natural Gd for neutrons, the magnetic structure was investigated by magnetic X-ray scattering [15]. The initial ordering of Gd occurs into a transversally polarized spin density wave with an incommensurate wave vector $q = (0.555,0,0)$. The direction of $q$ is along the $a$-axis with spins directed along $b$. At 14 K a $c$-axis component to the moment develops. The two components of the ordered magnetic moment along $b$- and $c$-axes feature the same wave vector ($q_a \approx 0.55a^*$). Depending on the relative phase shift $\Delta\phi$ between the two oscillations, two possible structures with $\Delta\phi = 0$ (transverse wave) and $\Delta\phi = \pi$ (helical structure) are compatible with the experimental data. The transverse wave would lead to a modulation of the magnetic moments which all make the same angle with respect to the $c$-axis. By contrast, the helical-like structure would give rise to a distribution of the size and orientation of the magnetic moments resulting in an elliptical projection onto the ($b$,$c$) plane.

The Mössbauer spectra recorded in the paramagnetic state (Fig. 1) are well represented by a pure quadrupolar splitting of axial symmetry with $e^2qQ = (+)5.38(2)$ mm s$^{-1}$ (its sign was determined from the spectra recorded in the ordered state) [16,17]. This allows us to estimate the second-order $B_2^0$ CEF parameter across the $RNi_2B_2C$ series because $e^2qQ$ is proportional to $B_2^0$ through the relation

$$B_2^0\,(\mathrm{K}) \approx -77.5\alpha_J\langle r^2\rangle(e^2qQ) \quad (1)$$

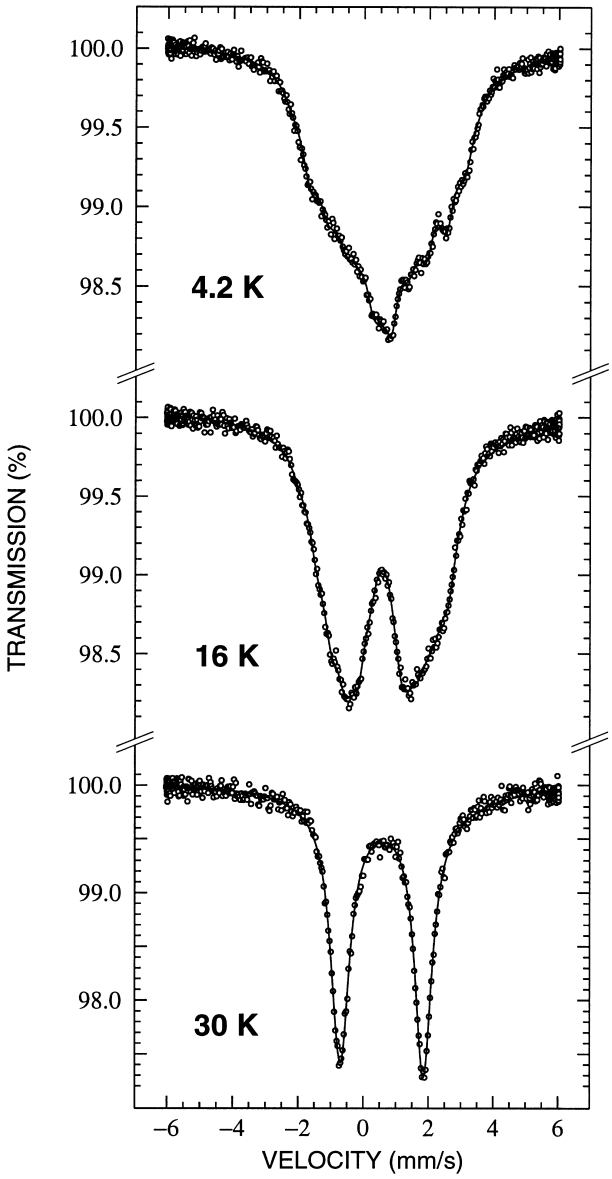


Fig. 1. $^{155}$Gd Mössbauer spectra of $GdNi_2B_2C$ recorded at 4.2 K (bunched helical structure), 16 K (squared transverse spin modulation) and 30 K (paramagnetic phase) [17].

Here, $\alpha_J$ is the Stevens factor, and $\langle r^2 \rangle$ is the second moment of the 4f electron radial wave function in $a_0^2$ units. $e^2qQ$ is expressed in mm s$^{-1}$.

Application of relation (1) to, for example, $HoNi_2B_2C$ leads to a $B_2^0$ value of 0.69 K, to be compared to the values of 0.85 and 0.37 K obtained from the analysis of magnetization (see Table 2 of Ref. [19]) and neutron [20] data, respectively. Although the agreement between the different estimates could be worse, which is the case for $ErNi_2B_2C$ [19,20], relation (1) nevertheless correctly predicts the sign of $B_2^0$.

If $B_2^0$ is the leading parameter of the crystal field Hamiltonian its sign determines the easy direction of magnetization, i.e. an easy axis when $B_2^0 < 0$ and an easy plane when $B_2^0 > 0$. From the positive sign found for $e^2qQ$ it is anticipated that the *R*-moments are parallel to the *c*-axis when $\alpha_J > 0$ (Er, Tm) and in the basal plane when $\alpha_J < 0$ (Pr, Nd, Tb, Dy, Ho). These predictions are nicely confirmed by the neutron diffraction data [13], except for the Er compound which exhibits a basal plane anisotropy owing to the interplay of higher-order CEF parameters [18].

The spectra recorded below 14 K can be approximated by assuming a single set of hyperfine parameters with $H_{hf}$ ($-26.3$ T at 4.2 K) making an angle $\theta$ of 56(2)° with the efg principal axis $V_{zz}$ which is along the *c*-direction [17]. Notice that the $\theta$ value is close to the magic angle (54°7) expected for a random orientation of Gd moments. This single set model turns out to be rather crude for representing the data taken between 14 K and $T_N$. The Mössbauer results taken together with the magnetic structure models deduced from magnetic X-ray diffraction experiments led to the following conclusions [17]. (a) From $T_N$ down to 14 K, the magnetic structure is modulated along *a* but the modulation should be squared (at least at 16 K) with the moments along *b* ($\theta = 90°$). (b) Below 14 K, the structure is helical ($\Delta\phi = \pi$), with the moments in (*b*,*c*) planes and propagation along *a*. The quality of the Mössbauer fit is significantly improved if bunching to the helix is introduced (the distribution of $H_{hf}$ becomes minute and the Gd moments are almost random with respect to the *c*-axis, $\langle\theta\rangle \approx 55°$, i.e. the projection of the moments onto the (*b*,*c*) plane becomes nearly a circle). It is worth pointing out that either squaring of the sine-modulation or bunching of the helix will result in the occurrence of higher harmonics. The spectra shown in Fig. 1 were actually reanalysed in the frame of the magnetic structure models described above and by introducing third- and fifth-order harmonics in the expressions describing the modulation of the magnetic moments [17]. Further magnetic X-ray or neutron scattering experiments should be devoted to the search for these harmonics.

### 3.2. $DyNi_2B_2C$

$^{161}$Dy Mössbauer effect measurements have been utilized to investigate the magnetic properties and the nature of the ground state of the $DyNi_2B_2C$ magnetic superconductor ($T_N \sim 11$ K, $T_C \sim 6$ K) [19]. The Mössbauer data shown in Fig. 2 indicate that the magnetic transition at ~11 K is of first order. This conclusion was inferred from the observation of a hyperfine field which is temperature independent, at least up to 10 K, and from the coexistence within a narrow temperature range of magnetically ordered and paramagnetic domains. The two samples that were investigated had different superconducting properties, but do show any significant difference in the hyperfine interaction parameters. The analysis of the hyperfine field and of the quadrupole coupling constant led us to conclude that the Dy moments of 9.8 $\mu_B$ are confined in the basal plane

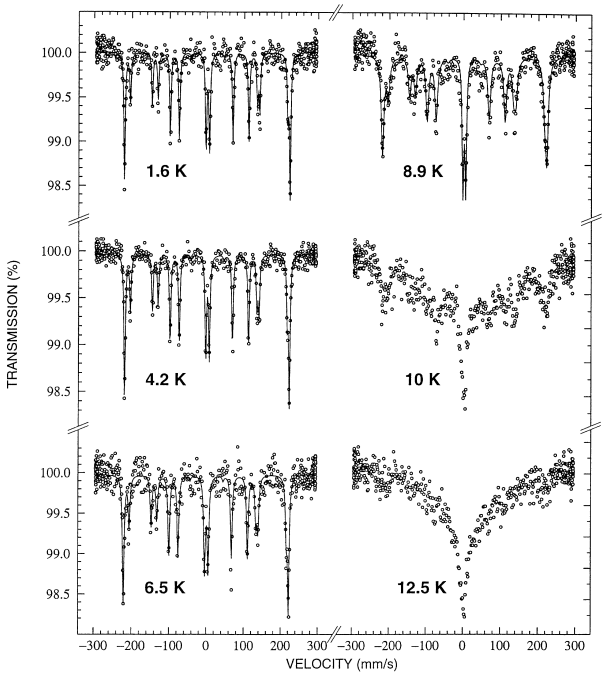


Fig. 2. $^{161}$Dy Mössbauer spectra of the magnetic superconductor $DyNi_2B_2C$ ($T_N \sim 11$ K, $T_C \sim 6$ K) recorded at different temperatures. The overall splitting is proportional to the hyperfine field (or Dy magnetic moment) [19].

and that $\langle J_z^2 \rangle \approx 54.6$ at saturation. The crystal field ground state of mainly $|\pm 1/2\rangle$ character ($B_2^0$ is positive and large; it amounts to about 2 K according to Eq. (1)) explains the direction of magnetization (basal plane) as well as the observed rather fast relaxation rate ($\Omega \sim 10^9$ Hz) of the Dy moments which results in the collapse of the magnetic hyperfine structure above $T_N$. Although the second-order $B_2^0$ CEF parameter plays a dominant role, it is necessary to include higher-order CEF terms (e.g., negative $B_4^0$) to account for the observed hyperfine interaction strengths and specific heat data. Indeed, by considering only the second-order CEF term, an unrealistic molecular field of 230 kOe (perpendicular to the CEF axis) is needed to account for the observed Dy moment (9.8 $\mu_B$). Another significant result of this Mössbauer study is that the isomer shift value ($-2.35(9)$ mm s$^{-1}$ vs. Dy metal) in $DyNi_2B_2C$ is closer to those in non-metallic Dy systems. This suggests that the Dy–C layer is basically a non-conducting layer which in turn implies that superconductivity arises from the Ni–B layer.

## 4. Mössbauer study of Dy/Fe multilayers

Much work has been devoted to R/Fe multilayers because of the potential magneto-optical applications. Perpendicular magnetic anisotropy (and perpendicular orientation of the magnetic moments) is strong even at RT in compositionally modulated amorphous R/Fe multilayers of small thickness ($< \sim 20$ Å) [21]. On the other hand, crystalline R/Fe multilayers of larger individual thickness are of theoretical interest because they may exhibit a reversible reorientation transition of the magnetic moments from the preferred in-plane orientation at high temperature to the preferred out-of-plane orientation at low temperature [22]. The reorientation temperature has been studied extensively by $^{57}$Fe Mössbauer spectroscopy [21,22]. In contrast, up to recently little was known about the spatial arrangement of *R*-magnetic moments in R/Fe multilayers and the correlation of the Fe-spin texture and the *R*-moments arrangement. The missing information was provided by a $^{57}$Fe and $^{161}$Dy Mössbauer investigation [23] of a Dy(48 Å)/Fe(40 Å) multilayer sample which contains bcc Fe layers exhibiting a reorientation transition.

One important result of the $^{57}$Fe Mössbauer study was the determination of the actual film structure of the investigated multilayer. It consists approximately of a sequence of ~22 Å thick bcc Fe layers, separated from ~34 Å thick hcp Dy layers by ~16 Å thick amorphous $Dy_{1-x}Fe_x$ interface alloy layers of probable concentration $x \approx 0.78$. The measured (4.2 K) average $^{161}$Dy hyperfine field (583 T), quadrupole coupling constant (109.4 mm s$^{-1}$) and isomer shift ($-0.1$ mm s$^{-1}$ vs. bulk Dy metal) are consistent with this model structure.

The other relevant information was provided by analysis of the spin-texture obtained from the relative intensities of six ($^{57}$Fe) and 16 ($^{161}$Dy) Mössbauer lines (Fig. 3). The relative line intensities yield values of the average $\langle \beta \rangle$ angle between the film normal direction and the direction of the hyperfine magnetic field (or Fe, Dy spin direction).

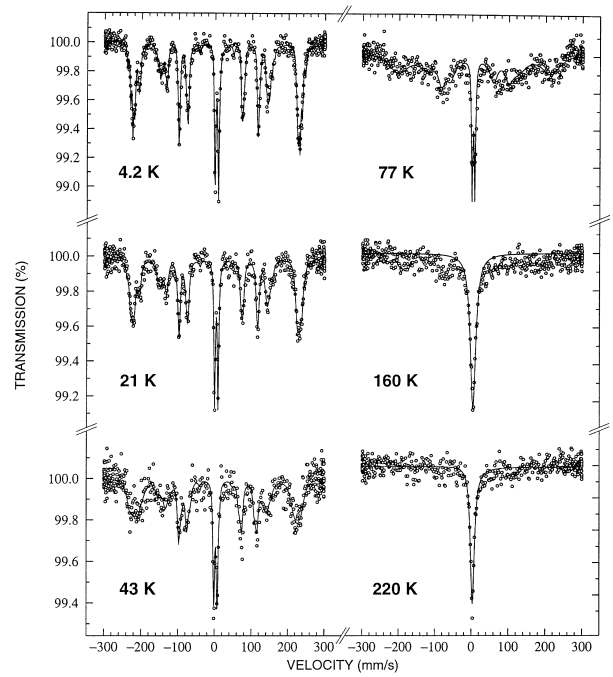


Fig. 3. Temperature dependence of the $^{161}$Dy Mössbauer spectra of a $[Dy(48\ Å)/Fe(40\ Å)]_{250}$ multilayer [23].

The bcc Fe layers in the present multilayer exhibit a broad *T*-dependent spin reorientation. The average $\langle\beta\rangle$ angle decreases from 73° on cooling at 300 K and saturates near a value of 52° below 100 K, which is the observed Curie temperature of the Dy layers (as inferred by SQUID magnetometry). This implies that at low temperature the Fe moments are on average either oriented, for instance, on a cone angle of 52°, or oriented nearly at random. Simultaneously, $\langle\beta\rangle$ for the hcp Dy layers at 4.2 K (55°) is also close to the magic angle of 54.7°. The reorientation transition of the magnetic moments is known to be the result of competition between the shape anisotropy energy (which favors the in-plane magnetization direction, i.e., $\beta=90°$) and the perpendicular surface or interface anisotropy energy which favors the perpendicular magnetization direction, i.e. $\beta=0°$. From the observed Fe and Dy textures at 4.2 K ($\beta\sim52°$ and 55°, respectively) it was concluded that due to the exchange coupling between Dy and Fe layers (via the amorphous interface) the nearly random spatial arrangement of the Dy moments in the hcp Dy layers induces a randomizing effect on the spatial Fe-spin arrangement which opposes the influence of the perpendicular interface anisotropy. This prevents the Fe moments from developing a stronger out-of-plane spin component at low temperature.

Finally, it is worth mentioning that the Fe and Dy layers do not order magnetically simultaneously. While the Fe layers are already ordered at RT, the Néel temperature of the Dy layers was estimated to be around 200(20) K from the temperature dependence of the $^{161}$Dy Mössbauer spectral shape (Fig. 3).

## 5. Mössbauer study of cubic $NpX_3$ compounds

The actinide compounds $AnX_3$, where X is an element from Group IIIA or IVA, crystallize in the cubic $AuCu_3$ structure. They are characterized by actinide separation far above the Hill limit, therefore 5f–ligand hybridization is the main mechanism responsible for the delocalization of the 5f electrons. The systematics of this hybridization have been well demonstrated for the $UX_3$ compounds which either do not order magnetically (X=Al, Si, Ge, Sn) or exhibit antiferromagnetism (X=Ga, In, Tl, Pb). It was concluded that the 5f–ligand hybridization increases as one moves up a column of the Periodic Table or moves from a Group IIIA element to a Group IVA element [24]. Data for the corresponding isostructural $NpX_3$ intermetallics were, until recently, much less documented owing to the necessity of handling these materials in specialized laboratories. The recent development in the early nineties of the single crystal fabrication of some members of this series at the CEA-Cadarache led to dramatic progress in our understanding of their properties [25] as inferred from Mössbauer spectroscopy (Figs. 4 and 5), neutron scattering and transport and magnetization measurements (Table 2).

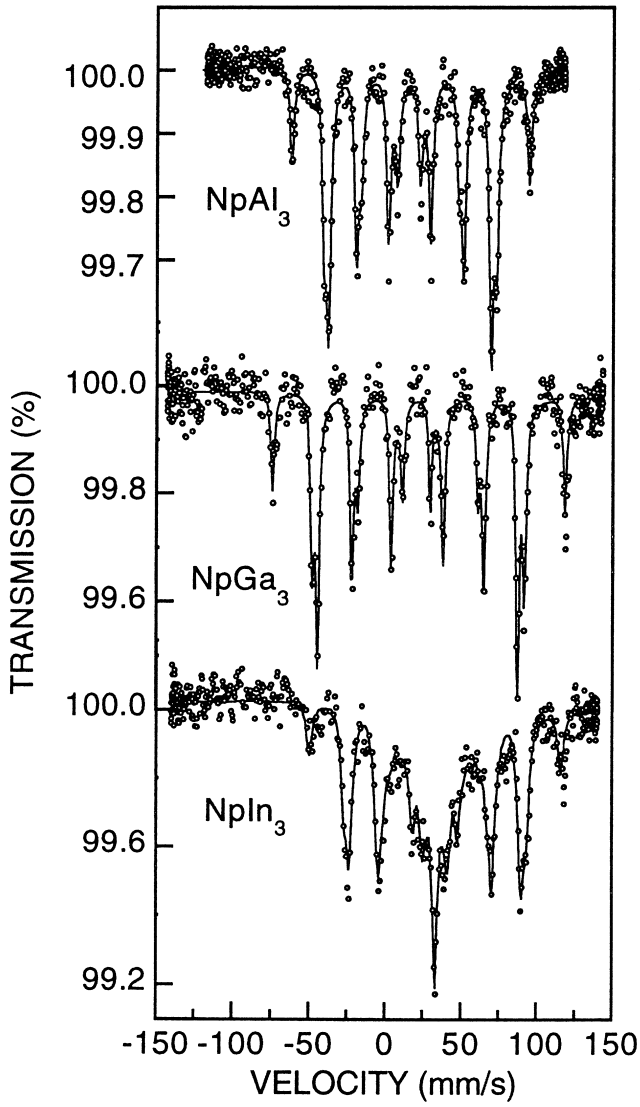


Fig. 4. $^{237}$Np Mössbauer spectra of $NpAl_3$, $NpGa_3$ and $NpIn_3$ at 4.2 K. Note the occurrence for the latter compound of a central line (zero-field component) which indicates that about 10% of the Np ions do not carry a magnetic moment [26,30].

### *5.1. Np charge state and delocalization of the 5f electrons in $NpX_3$*

Table 2 and Fig. 6 show that the isomer shifts for the $NpX_3$ series span a rather large range of values. Actually, the $\delta_{IS}$ lie between those corresponding to the most ionic $Np^{3+}$ ($+37$ mm s$^{-1}$) and ionic $Np^{4+}$ ($-9$ mm s$^{-1}$) compounds [1,2]. As discussed previously the presence of conduction electrons increases $\rho(0)$. This shifts $\delta_{IS}$ to the next highest charge state in Np intermetallics (i.e. $Np^{3+}\rightarrow Np^{4+}$). From these observations it may be anticipated that, for a given charge state, the isomer shift for an intermetallic compound should be smaller than the value corresponding to the most ionic compound. Thus accord-

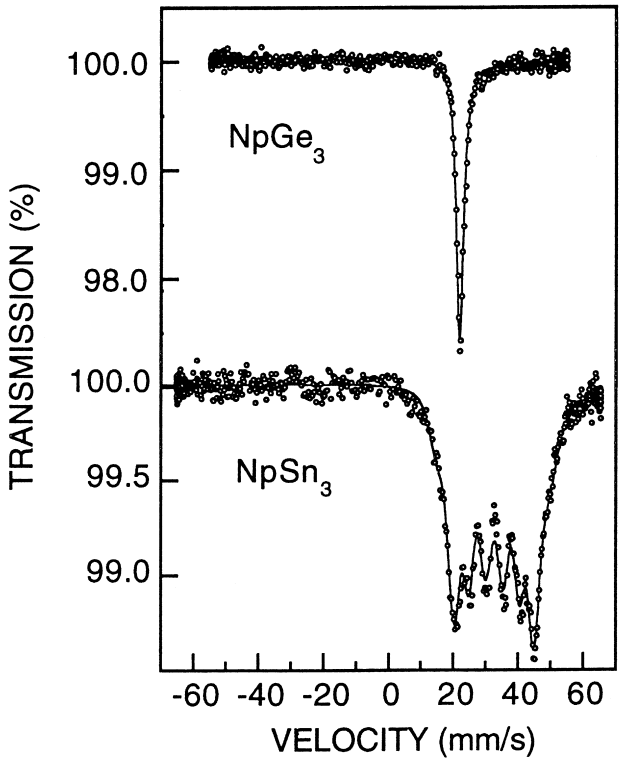


Fig. 5. $^{237}$Np Mössbauer spectra of $NpGe_3$ and $NpSn_3$ at 4.2 K [29,32].

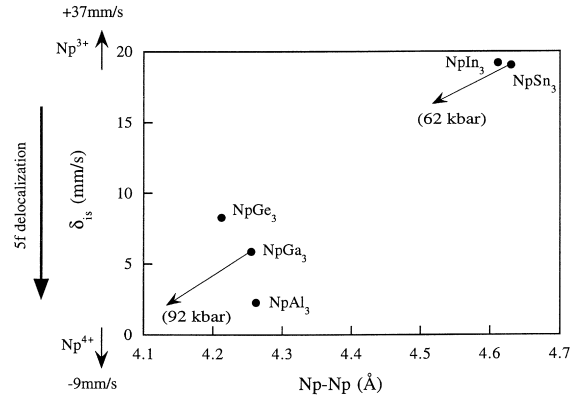


Fig. 6. Dependence of the isomer shift on the Np–Np separation for the $NpX_3$ series. The arrows show the variation of $\delta_{IS}$ under applied pressures [25].

ing to these $\delta_{IS}$ systematics we may safely assign a $Np^{3+}$ charge state for the Np ions in the $NpX_3$ series.

The change of $\delta_{IS}$ within the $NpX_3$ series may be ascribed either to a volume effect (increase of $\rho(0)$ due to compression of the 6s-shell with decreasing lattice parameter) or to increasing hybridization effects, i.e. 5f delocalization with decreasing lattice parameter (the screening of the s electrons by the 5f electrons decreases). Actually, the volume dependence of the isomer shift in $NpSn_3$ [31] and $NpGa_3$ [33] shows that the large span of $\delta_{IS}$ cannot be explained by volume effects alone (this seems at least to be the case for $NpGa_3$ and $NpAl_3$).

Although the volume dependence of the hyperfine parameters ($H_{hf}$, $\delta_{IS}$) and the ordering temperature for $NpSn_3$ [31] are clearly typical of localized 5f electron systems, the high pressure behaviour of $NpGa_3$ indicates a weak delocalization of the 5f electrons [33]. $NpX_3$ compounds should be viewed as narrow f-band compounds. Finally, $NpAl_3$, which has the smallest isomer shift, should be a good candidate for further high pressure studies.

### 5.2. Ground state of the $Np^{3+}$ ions in $NpX_3$

Both the hyperfine field (or the Np ordered moment) and the quadrupole coupling constant for ordered $NpX_3$ compounds are strongly reduced with respect to the free-ion $Np^{3+}$ values of 530 T (or 2.57 $\mu_B$) and $-27.3$ mm s$^{-1}$, respectively (Table 1). Except for $NpSn_3$, most of this reduction may be accounted for by crystal field interaction acting on the $^5I_4$ ground state multiplet of the $Np^{3+}$ ions ($5f^4$). In a cubic crystalline electric field (CEF), the $^5I_4$ state splits into a singlet $\Gamma_1$ (non-magnetic), a non-Kramers doublet $\Gamma_3$ (non-magnetic) and two triplets $\Gamma_4$ and $\Gamma_5$ (magnetic). Note that according to the Lea, Leask and Wolf diagram, $\Gamma_4$ cannot be the ground state unless the $x$ parameter (ratio between the fourth- and sixth-order CEF terms) is equal to 0.837 [32].

At low temperature, the exchange interaction removes

Table 2
Magnetic and electronic properties of $NpX_3$ intermetallic compounds: F = ferro or ferrimagnet, AF = antiferromagnet, PP = Pauli paramagnet, SF = spin fluctuator, $m_0$ is the saturated ordered moment as inferred from Mössbauer measurements, the values of $H_{hf}$ and $e^2qQ$ are those measured at 4.2 K

| Compound | Type of magnetic order | $T_N$, $T_C$ (K) | $H_{hf}$ (T) | $m_0$ ($\mu_B$) | $\delta_{IS}^a$ (mm s$^{-1}$) | $e^2qQ$(mm s$^{-1}$) | Ref. |
|---|---|---|---|---|---|---|---|
| $NpAl_3$ | AF II | 37 | 292(1) | 1.36(5) | 2.6(1) | −2.2(2) | [26] |
| $NpGa_3$ | AF II/F | 65/50 | 335(3) | 1.56(5) | 5.9(1) | −2.9(4) | [27,28] |
| $NpIn_3$ | F/F/AF | 13.5/10/8.2 | 300(3)[b] | 1.40(5)[b] | 19.3(2) | −2.0(5) | [29,30] |
| $NpGe_3$ | PP, SF | | | | 8.0(1) | 0 | [29] |
| $NpSn_3$ | AF I | 9.5 | 66(2) | 0.30(2) | 19.0(2) | 0.0(5) | [31,32] |

[a]Relative to $NpAl_2$.
[b]Maximum value of the modulated hyperfine field or magnetic moment.

the degeneracy of the CEF states. It turns out that for the $\Gamma_5$ level the calculated (intermediate coupling scheme) ordered moment ($1.6\,\mu_B$) and quadrupole coupling constant ($-3.9\,\mathrm{mm\,s^{-1}}$) are very close to the experimental value for $NpAl_3$, $NpGa_3$ and $NpIn_3$. It should be noted that within the CEF model the absence of a local Np moment in $NpGe_3$ can be accounted for by assuming a $\Gamma_1$ ground state. On the other hand, an exchange mixing of the $\Gamma_1$ ground state with an excited $\Gamma_4$ state could also be invoked to explain the small moment ($0.3\,\mu_B$) and the almost vanishing $e^2qQ$ value observed for $NpSn_3$. An alternative and most probable explanation, as suggested by resistivity and susceptibility data [29], would be that both $NpSn_3$ and $NpGe_3$ are Kondo lattice where the moment originating from the $\Gamma_5$ level is partially (or totally) quenched by the conduction electrons. We expect that planned inelastic neutron scattering experiments will shed more light on the actual nature of the ground state of $NpSn_3$.

The variation of the magnetic properties within the $NpX_3$ series shows similarities but also some differences to the trend observed in the $UX_3$ counterparts. As a matter of fact the Np compounds appear to be more magnetic, for example there is no breakdown of magnetic order in Group IIIA and in Group IVA. $NpSn_3$ is already magnetic while $NpGe_3$ is close to the boundary of the magnetic–nonmagnetic transition. On the other hand, the magnetic moment remains almost constant in the $NpX_3$ series with IIIA elements while *m* decreases when moving up the X column in the corresponding $UX_3$ compounds.

## References


[1] B.D. Dunlap, G.M. Kalvius, in: A.J. Freeman, G.H. Lander (Eds.), Handbook on the Physics and Chemistry of the Actinides, Vol. 2, North-Holland, Amsterdam, 1985.

[2] W. Potzel, G.M. Kalvius, J. Gal, in: K.A. Gschneidner, Jr., L. Eyring, G.H. Lander, G.R. Choppin (Eds.), Handbook on the Physics and Chemistry of Rare Earths, Vol. 17, North-Holland, Amsterdam, 1993.

[3] B. Coqblin, The Electronic Structure of Rare-earth Metals and Alloys: The Magnetic Heavy Rare-earths, Academic Press, London, 1977.

[4] J. Jensen, A.R. MacKintosh, Rare-earths Magnetism, Clarendon Press, Oxford, 1991.

[5] A.J. Freeman, G.H. Lander (Eds.), Handbook on the Physics and Chemistry of the Actinides, Vols. 1 and 2, North-Holland, Amsterdam, 1984, 1985.

[6] K.A. Gschneidner, Jr., L. Eyring, G.H. Lander, G.R. Choppin (Eds.), Handbook on the Physics and Chemistry of Rare Earths, Vols. 17 and 19, North-Holland, Amsterdam, 1993 and 1994.

[7] A. Hiess, M. Bonnet, P. Burlet, E. Ressouche, J.P. Sanchez, J.C. Warenborgh, S. Zwirner, F. Wastin, J. Rebizant, G.H. Lander, J.L. Smith, Phys. Rev. Lett. 77 (1996) 3917.

[8] A. Hiess, F. Bourdarot, P. Burlet, E. Ressouche, J.P. Sanchez, F. Wastin, J. Rebizant, E. Suard, G.H. Lander, Phys. Rev. B 55 (1997) 1138.

[9] P. Bonville, B. Canaud, J. Hammann, J.A. Hodges, P. Imbert, G. Jéhanno, A. Severing, Z. Fisk, J. Phys. I (France) 2 (1992) 459.

[10] P. Bonville, P. Bellot, J.A. Hodges, P. Imbert, G. Jéhanno, G. Le Bras, J. Hammann, L. Leylekian, G. Chevrier, P. Thuéry, L. D'Onofrio, A. Hamzic, A. Barthélémy, Physica B 182 (1992) 105.

[11] K. Drescher, M.M. Abd-Elmeguid, H. Micklitz, J.P. Sanchez, Phys. Rev. Lett. 77 (1996) 3228.

[12] I. Nowik, Hyperfine Interactions 13 (1983) 89.

[13] J.W. Lynn, S. Skanthakumar, Q. Huang, S.K. Sinka, Z. Hossain, L.C. Gupta, R. Nagarajan, C. Godard, Phys. Rev. B 55 (1997) 6584, and references therein.

[14] P.C. Canfield, B.K. Cho, K.W. Dennis, Physica B 215 (1995) 337.

[15] C. Detlefs, A.I. Goldman, C. Stassis, P.C. Canfield, B.K. Cho, J.P. Hill, D. Gibbs, Phys. Rev. B 53 (1996) 6355.

[16] F.M. Mulder, J.H.V.J. Brabers, R. Coehoorn, R.C. Thiel, K.H.J. Buschow, F.R. de Boer, J. Alloys Comp. 217 (1995) 118.

[17] K. Tomala, J.P. Sanchez, P. Vulliet, P.C. Canfield, A. Winiarska, Z. Drzazga, Phys. Rev. B (submitted).

[18] P. Bonville, J.A. Hodges, C. Vaast, E. Alleno, C. Godart, L.C. Gupta, Z. Hossain, R. Nagarajan, G. Hilscher, H. Michor, Z. Phys. B 101 (1996) 511.

[19] J.P. Sanchez, P. Vulliet, C. Godart, L.C. Gupta, Z. Hossain, R. Nagarajan, Phys. Rev. B 54 (1996) 9421.

[20] U. Gasser, P. Allenspach, F. Fauth, W. Henggeler, J. Mesot, A. Furrer, S. Rosenkranz, P. Voderwisch, M. Buchgeister, Z. Phys. B 101 (1996) 345.

[21] T. Shinjo, Surf. Sci. Rep. 12 (1991) 49.

[22] T. Shinjo, K. Mibu, S. Ogawa, N. Hosoito, in: B.T. Jonker, J.P. Heremans, E.E. Marimero (Eds.), Growth, Characterization and Properties of Ultrathin Magnetic Films and Multilayers, MRS Symposia Proceedings No. 151, Materials Research Society, Pittsburgh, 1990.

[23] J. Tappert, W. Keune, R.A. Brand, P. Vulliet, J.P. Sanchez, T. Shinjo, J. Appl. Phys. 80 (1996) 4503.

[24] D.D. Koelling, B.D. Dunlap, G.W. Crabtree, Phys. Rev. B 31 (1985) 4966.

[25] J.P. Sanchez, E. Colineau, in: K. Tomala, E. Görlich (Eds.), Proceedings of XXX Zakopane School of Physics: Condensed Matter Studies by Nuclear Methods, Institute of Physics, Jagiellonian University, Institute of Nuclear Physics, Krakow, 1995.

[26] J.L. Oddou, R.R. Arons, A. Blaise, P. Burlet, E. Colineau, C. Jeandey, E. Ressouche, J.P. Sanchez, J. Larroque, J. Rebizant, J.C. Spirlet, J. Magn. Magn. Mater. 135 (1994) 183.

[27] M.N. Bouillet, T. Charvolin, A. Blaise, P. Burlet, J.M. Fournier, J. Larroque, J.P. Sanchez, J. Magn. Magn. Mater. 125 (1993) 113.

[28] E. Colineau, F. Bourdarot, P. Burlet, J.P. Sanchez, J. Larroque, Physica B 230–232 (1997) 773.

[29] J.P. Sanchez, M.N. Bouillet, E. Colineau, A. Blaise, M. Amanowicz, P. Burlet, J.M. Fournier, Physica B 186–188 (1993) 675.

[30] E. Colineau, A. Blaise, P. Burlet, J.P. Sanchez, J. Larroque, Physica B 206–207 (1995) 528.

[31] G.M. Kalvius, S. Zwirner, U. Potzel, J. Moser, W. Potzel, F.J. Litterst, J. Gal, S. Fredo, I. Yaar, J.C. Spirlet, Phys. Rev. Lett. 65 (1990) 2290.

[32] T. Charvolin, A. Blaise, M.N. Bouillet, P. Burlet, J.M. Fournier, J. Larroque, J. Rossat-Mignod, J.P. Sanchez, J. Magn. Magn. Mater. 132 (1994) 46.

[33] S. Zwirner, V. Ichas, D. Braithwaite, J.C. Warenborgh, S. Heathman, W. Potzel, G.M. Kalvius, J.C. Spirlet, J. Rebizant, Phys. Rev. B 54 (1996) 12283.